TÜBİTAK
ACADEMIC JOURNALS
Published by the Scientific and Technological Research Council of Turkey

TURKISH JOURNAL OF ELECTRICAL ENGINEERING AND COMPUTER SCIENCES –ISSN NO. 13000632 (SCOPUS INDEX)

Machine learning algorithm-based Fusion of Hyperspectral and 3D Laser Scanning Images

Shanthi T [1], Anand R[2] , Vivek Karthick[3] and Veni S[4],

[2] Research Scholar, Department of Electronics and Communication Engineering, Amrita School of Engineering, Coimbatore, Amrita Vishwa Vidyapeetham, India and Assistant Professor, Research Member in Sona SIPRO, Department of ECE, Sona College of Technology, Salem. Email: anand.r@sonatech.ac.in

[1] Assistant Professor, Research Member in Sona SIPRO, Department of ECE, Sona College of Technology, Salem shanthi@sonatech.ac.in.

[3] Assistant Professor, Research Member in Sona SIPRO, Department of ECE, Sona College of Technology, Salem

[4]Department of Electronics and Communication Engineering, Amrita School of Engineering, Coimbatore, Amrita Vishwa Vidyapeetham, India.

Abstract—Data fusion on remote sensing refers to the process of combining data from multiple Sensors to produce a dataset. The resulted data set contains more detailed information then each of the individual sources also data from multiple sensors can significantly improve the accuracy and interpretation of features. Pixel-level, Feature-level and Decision-level are three common levels of data fusion. Here, we summarized the proposal work, to increasing the testing samples and reduce the computational complexity of processing input image. Generally, spectral resolution will give more about information of the spectrum of the image and LiDAR gives the light intensity if the image. The Novelty of this work to reduce the training samples and achieve better classification accuracy in urban places. This work, concentrates on the subsequent intentions: (i) To enhance the classification precision in HSI and LiDAR images (ii) To lessen the assorted pixels in suburban constructions that are encircled by tiny trees (iii) To reduce the comparable pixels of streets and parking areas. Here, 15 separate classes were categorized which are significant for the expansion in urban areas.

I. INTRODUCTION

In 2019, the first time in history, more than half the world's population lives in cities. Key objectives of this proposed contribution is grouping of LiDAR (Spectral resolution) and HSI (Spatial resolution) for urban area land-use arrangement. The Importance of Hyperspectral Image (HSI) has accurate discrimination of different materials in spectral resolution and analysis a small spatial structures in spatial resolutions. Both Spatial and Spectral resolution are powerful tool for accurate analysis of the earth. LiDAR data provides useful information related to size, structure and elevation. So, the fusion of hyperspectral and LiDAR has good impact to classifiy different urban areas. Fusion of HSI and LiDAR provides a complementary information because hyperspectral image has spectral information but elevation of the image is not available, but LiDAR has elevation of the image but no spectral information. The classifier should be accurate, automatic and simple fast for fusion data [1], [2]. Big data procedures are deadly procedure in case of HSI image, let x be an input

attributes, and let $f(x)$ be a projecting or mapping function, which is shown in below,

$$y = f(x) \quad (1)$$

Data investigation must usually adapt only similar design, i.e., $x = x1, x2, , x3, . , . , xN$, which is, in between a enormous set of attributes x to N lesser attributes of sample[3].

II. LITERATURE SURVEY

HSI expertise has been more expressively used in past few years. Spectral- spatial classification is conventional spectral classifiers, consider hyperspectral images as a list of spectral dimensions with no spatial informations. The increases of labelling uncertainty, it may overcome by using combination of spectral and spatial information[4]. Attributes filters operate only on the connected Some of the research works performed on LiDAR data alone includes involuntary Structure of Edifice paths, Separation of 3D LIDAR[5].

In Ancient years, the scholars are used to share the information by using palm leaf images. Narahari Sastry Panyam [4], describes the 3D-feature (depth of indentation) which is directly proportional to the pressure applied to scriber at the point for character Road Accident Detection using Convolutional Neural Network recognition. Narahar i Sastr y and et.al have used Two Dimensional - Discrete wavelet transform (2D-DW T), Fast Fourier transform (2D-FFT) for extracting features from printed manuscripts. A total of 1540 images with 1232 in training and 308 in testing have been outlined in the work. The authors have utilized a two-level transforms and this transfor m helps to improve accuracy up to 96.4%. H. Swethalakshmi [6], has made use of the sequence of strokes in Telugu and Devanagiri characters and the ectracted features are used to classify these characters by using Support Vector Machine (SVM). The palm-leaf manuscript character images that are fed into the proposed approach were normalization, smoothen and interpolated. Saeeda Naz [7], has approached an implied segmentation based optical recognition system for Urdu Character in Nastlaliq Scripts. A prediction rate of 96.40% was achieved by the proposed method. Apurva A. Desai [3] have used a neural network type of classification and compared it with other machine learning approaches. This literature shows that neural network based approach gives a better result when compared to other approaches. Apurva A. Desai has done this comparison with Gujarathi Characters Hidden Markov Model and fuzzy logic algorithm was used on Urdu scripts by Muhammad Imran Razzak [8] for character recognition. The approach was evaluated on Nastaliq and Nasakh script-based languages. With around twenty-six time-invariant features and statistical features, the approach provided 87.4% and 74.1% of accuracy for Nastaliq and Nasakh scripts respectively. An effective optical character recognition system to recognize and identify the Persian character using Support vector machine (SVM) was proposed]. In this work, we addressed to overcome those problem by using fusion of spectral and spatial components for detecting urban objects. The upcoming sections: Section (3) deals with summary of hyperspectral image and LiDAR. Section (4) describes the proposed methodology by continuing the Section (5) elaborates the proposed method for multi-class Non-Linear SVM polynomial kernel classification techniques are reviewed in section and end up with the Conclusions and future scope this work.

III. OVERVIEW OF HYPERSPECTRAL AND LIDAR

HSI Sensor is extremely helpful than any other sensor because it provides a constant band in the range, which can be helpful for identifying precise objects covering in a scene [13], [14],[15]. LiDAR processing: In most topographical data, advancement information is deadly component.

A. Research zone and Research volume

The HSI image were taken at campus of Houston and nearby metropolises of Texas. Information assortment is about 4 km^2, which is exposed in figure 1 and 2 for both HSI and DSM resulting from LiDAR [18].

Fig. 1: Airborne Houston Campus Hyperspectral Image

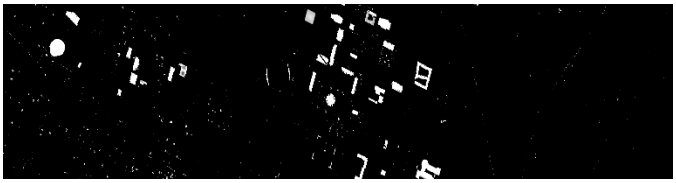

Fig. 2: Airborne Houston Campus DSM

LiDAR information has 2.5 three-dimensional purposes [19].

IV. METHODOLOGY

The procedure for urban land-use and urban land protection arrangement of fusion of HSI image & LiDAR are: (i) Image preprocessing (ii) Dimensionality reduction using Minimum Noise friction (iii) Combine HSI and LiDAR using Pixel level (iv) Machine learning Classification (v) Calculating performance metrices like Kappa Coefficient and Accuracy. The Proposed flow graph of this effort is shown in Figure 3.

A. *Pre-Processing*

In Airborne HSI and LiDAR image is needed, atmospheric adjustment is not required very much since the picture was taken by CASI and the elevation of sensor is only 1676.4 meter above the base level [20]. ,[21]. Fusion of HSI and LiDAR information provides the data size of 349*1905*145 (9,64,02,525 pixels).

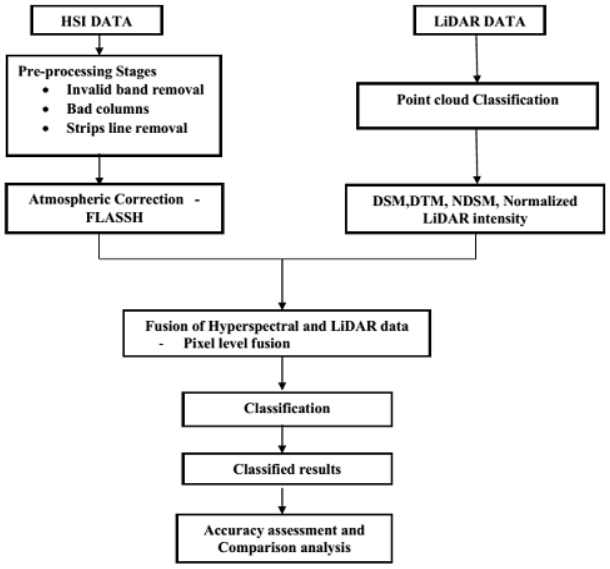

Fig. 3: Flow chart of Proposed Method

Throughout imagining viewpoint, the 3-D information can be altered to 2-D information. Conclusively, the data size fused information becomes (145*6,64,845 pixels [22], [23] which is shown in Table 1.

Table 1: Quantity of the HIS, LiDAR and Combination of HSI and LiDAR

Size of the HSI	349x1905x144
Size of LiDAR	349x1905x1
Fusion of both HSI and LiDAR	349x1905x145

B. *PCA or MNF*

The benefits of Principal Component analysis (PCA) is to drop the unwanted dimensionality of any data and it has the property of orthogonality to each other which is shown in equation 2.

$$Z_j = a_i^T x$$

where $i = 1, 2, p$, every Principle Component (PC) denotes P, it's a direct mixture of x. Initial PC is a_1^T exposed to $a_1^T a_1 = 1$ i.e., maximum variability of $a_1^T x$. Second PC is $a_2^T x$ is maximum variability of $a_2^T x, a_1^T x$ and it is subjected to $a_2^T a_2 = 1$ and $cov(a_2^T x, a_1^T x)$ and if we have maximum variables with constraint as $a_j^T a_j = 1$ to be computed [24], [25] & [26] used in this work.

C. *Pixel Level Fusion for HSI and LiDAR*

Steps for combine of HSI and LiDAR data is explained as follows: (i) Gathering of HSI and LiDAR data. (ii) Elimination of illegal wavelength of HSI data (iii) Fusion of HIS and LiDAR data by using Pixel level algorithm[27]. (v) Using Supervised Based algorithm to classify the fused data. The subsequent unit defines our projected prototypical using SVM [28].

V. PROPOSED METHOD

Classification problems are an essential category of difficulties in analytics in which the outcome changing or response variable takes separate classes. Primary objective of a classification model is to predict the probability of an observation belonging to a class, known as class probability [29]. Machine learning is a set of algorithms that have the capability to learn to perform tasks such as predication and classification effectively using data [33].

Nonlinear SVM is used for HSI data alone and for the combined data of HSI and LiDAR we use supervised learning . That let us to discover that Nonlinear SVM out goes well in terms of precision and Kappa measurement. In linear classifier, it may simply minimize the number of misclassification whilst maximizing the margin with respect to the correctly classified. In these the SVM training algorithm allows a training error. The hyperplane in feature space corresponding to a highly non-linear separating surface in the original input vector, hence this classifier is called a nonlinear classifier.

Fig. 4: Training ROIs

A. *Multi class Support Vector Machine*

Supervised machine learning classification algorithm needs a training samples with labels [30], The original HSI and LiDAR

data are shown in Figure 4 and 5. The training information are categorized to 15 dissimilar labels [33].

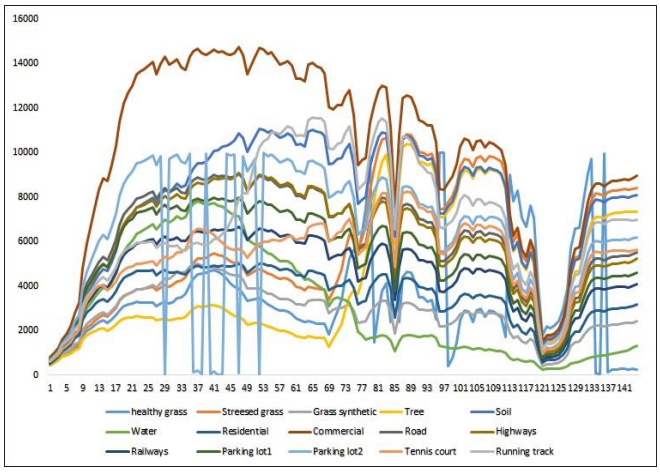

Fig. 5: Spectral separability of the different Training ROIs

If big data can be characterized in hyperplane overlay which is shown in below equation 3,

$$y_i(w^T x_i + b) \geq 1 \qquad (3)$$

Where, w is the load vector, x is input and b is the bias [31]. If $x_i \in C_i$ where i is the amount of labels. User can also assign labels belongingness, which is shown in equation 3. In case of non -separable case, the classes become overlap to each other's.). For non -separable case, the classes become overlap to each other's so we utilize the Lagrangian constraints $y_i(w^T x_i + b) \geq 1$ where i=1, 2...M, cannot be satisfied for all data points. To overcome this constraint will attempt to increase the Lagrangian to arbitrarily large values. These ideas are incorporated into the optimal margin algorithm described for the linearly separable case by introducing slack variable ϵ_i , where i = 1, 2, ..M , $\epsilon \geq 0$, into the constraints as shown in equation 4

$$\begin{aligned} y.x + b &\geq +1 - \epsilon_i, d_i = +1 \\ y.x + b &\geq -1 + \epsilon_i, d_i = -1 \end{aligned} \qquad (4)$$

Where, $\phi(x)$ is the mapping function could be done using an immeasurable amount of feature variables. The feature variables $\phi(x)$ in place of x which is describes below equation 5,

$$\mathrm{y(x)} = \mathrm{sign}\left(\sum_{i=1}^{15} \lambda_i d_i\left(\phi(x).\phi(x_i)\right) + W\right) \qquad (5)$$

Conclusively working summary of the SVM procedure is clarified below:

Step 1: A training information $\tau = 398907$ i.e, 60% of 664845 original images which is previously described and 40% of 664845 data points are used as testing samples data points $X_k = 15$ and anticipated output vector $d_k = [+1, -1]$.

Step 2: Select Polynomial Kernels and calculate dot product of $\varphi(x_j)^T \varphi(x_j)$

Step 3: Find LaGrange Multipliers.

Step 4: Classify the test data points to get the output of y(x).

B. *Accuracy Assessment*

Accuracy evaluation is founded on the confusion matrix which is several mixed data points are in same labels and the Accuracy Index (AI) and Kappa measurement [34]. Both kappa measurement and AI are shown in equations 11 and 12,

$$AI = \left[\frac{n - (omission + commision)}{n}\right] * 100 \qquad (10)$$

$$\mathrm{K} = \frac{N \sum_i^r x_{ii} - \sum x_i(x_{i+1})}{N^2 - \sum x_i(x_{i+1})} \qquad (11)$$

Where, 'n' is the number of confusion matrix, 'K' is the kappa measurement, 'r' is the amount of rows and N is the total of datapoint or Region of interest.

VI. Results and Discussion

Figure 6, 7 shows, all observations of class 1 to 15 are displayed in different colors. The hyperplane is the decision boundary how new observations are classified. The kernel calculates internal product among the different labels from 1 to 15. In table 2 shows, the accuracy has been improved from 67.12% to 79.55%) using SVM.

The individual classes are shown in figure 8. Table 2 shows the performance comparison of Nonlinear SVM on HSI and combined data (HSI + LiDAR) in terms of accuracy indexes.

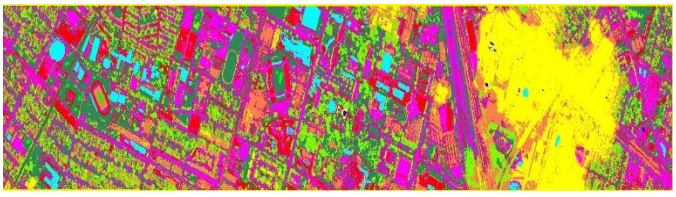

Fig. 6: HSI Image classification using SVM classifier

Fig. 7: HSI and LiDAR image classification using SVM classifier

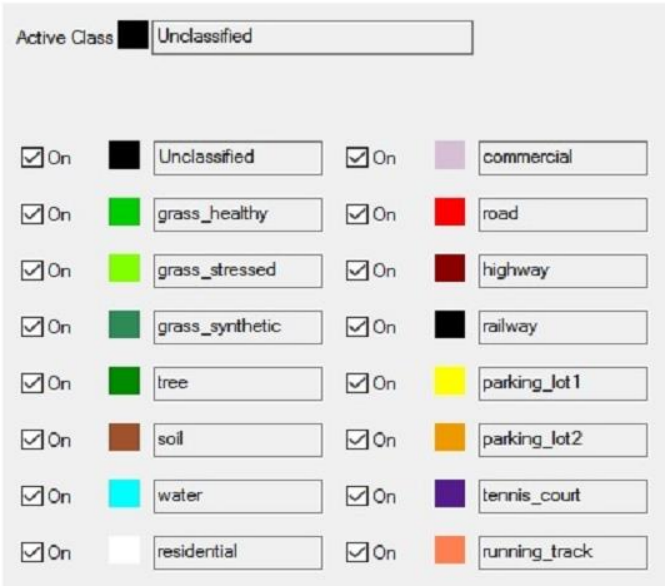

Fig. 8: Different color description for 15 different labels

The tasks which can be attained in remote sensing while fusion of HSI and LiDAR comprises rebuilding of items, ornamental feature origin and classification of classes [32][36],[37]. The land-use organization assistances to overcome the difficulties related to overflows and water in the urban areas [35],[38].

TABLE 2: The Overall Accuracy using Multi class SVM

Method	Overall Accuracy	Kappa coefficient	Computational Time
Nonlinear SVM for HSI alone	67.33	0.6432	16.47s
Nonlinear SVM for HSI and LiDAR	79.55	0.7789	14.32s

V. CONCLUSION

In this paper, we used Polynomial kernel based SVM collaborative systems can attain good kappa coefficient and accuracy for fusion of HSI and LiDAR. . This types the SVM-based fusion of HSI and LiDAR data classification method more relevant applications for Urban land use classification, that needs as low computational complexity in deployment level. For SVM classification, we used gradient descent procedure for training one-vs-all 15-class SVM classifiers. The gradient descent procedure is to accomplish of commerce with terabytes of training image and unites very quick-typically 100 iterations are enough. As a outcome, we achieve state-of-the-art performance on the SVM 15 class classification, i.e., 79.55% in classification accuracy and 0.6432 as Kappa coefficient.

REFERENCES

[1] Ammu, N.,& Irfanuddin, M. (2013). Big Data Challenges. International Journal of Advanced Trends in Computer Science and Engineering, 2(1),613-615.

[2] Laney, D. (2001). 3D data management: Controlling data volume, velocity and variety. META Group Research Note, 6, 70.

[3] Shafri, Helmi ZM, et al. Hyperspectral remote sensing of urban areas: an overview of techniques and applications. Research Journal of Applied Sciences, Engineering and Technology 4.11 (2012): 1557-1565.

[4] Ramdani, F. (2013). Urban vegetation mapping from fused hyperspectral image and LiDAR data with application to monitor urban tree heights.

[5] Zhang, K., Yan, J., & Chen, S. C. (2006). Automatic construction of building footprints from airborne LIDAR data. IEEE Transactions on Geoscience and Remote Sensing, 44(9), 2523-2533.

[6] Chen, Z., Xu, B., & Gao, B. (2016). An Image-Segmentation-Based Urban DTM Generation Method Using Airborne Lidar Data. IEEE Journal of Selected Topics in Applied Earth Observations and Remote Sensing, 9(1), 496-506.

[7] Nielsen, A. A. (2011). Kernel maximum autocorrelation factor and minimum noise fraction transformations. IEEE Transactions on Image Processing, 20(3), 612-624.

[8] Debes, Christian, et al. Hyperspectral and LiDAR data fusion: Outcome of the 2013 GRSS data fusion contest. IEEE Journal of Selected Topics in Applied Earth Observations and Remote Sensing 7.6 (2014): 2405-2418.

[9] Jung, A., Kardevn, P., & Tkei, L. (2005). Detection of urban effect on vegetation in a less built-up Hungarian city by hyperspectral remote sensing. Physics and Chemistry of the Earth, Parts A/B/C, 30(1), 255-259.

[10] Lulla, V. (2009). Hyperspectral applications in urban geography. In Planning and Socioeconomic Applications (pp. 79-86). Springer Netherlands.

[11] Man, Q., Dong, P., & Guo, H. (2015). Pixel-and feature-level fusion of hyperspectral and lidar data for urban land-use classification. International Journal of Remote Sensing, 36(6), 1618-1644.

[12] Schlkopf, B., Smola, A., & Mller, K. R. (1997, October).

Kernel principal component analysis. In International Conference on Artificial Neural Networks (pp. 583-588). Springer Berlin Heidelberg.
[13] Lillesand, T., Kiefer, R. W., & Chipman, J. (2014). Remote sensing and image interpretation. John Wiley & Sons.
[14] DellAcqua, F., et al. Exploiting spectral and spatial information in hyperspectral urban data with high resolution. IEEE Geoscience and Remote Sensing Letters 1.4 (2004): 322-326.
[15] Eismann, M. T. (2012, April). Hyperspectral remote sensing. Bellingham: SPIE.
[16] Targ, R., Steakley, B. C., Hawley, J. G., Ames, L. L., Forney, P., Swanson, D., ... & Calloway, R. S. (1996). Coherent lidar airborne wind sensor II: flight-test results at 2 and 10 m. Applied optics, 35(36), 7117- 7127.
[17] Huang, Z. W., He, S., & Qiu, L. (2012). The urban objects classification based on LiDAR 3D. In Applied Mechanics and Materials (Vol. 226, pp. 1840-1843). Trans Tech Publications.
[18] Du, Qian, and Saurabh PraSaD. Report on the 2013 IEEE GRSS data fusion contest: Fusion of hyperspectral and LiDAR data. (2013).
[19] htt p : //hyperspectral.ee.uh.edu/?pageid = 459
[20] Berger, C., Voltersen, M., Eckardt, R., Eberle, J., Heyer, T., Salepci, N., ... & Bamler, R. (2013). Multi-modal and multi-temporal data fusion: Outcome of the 2012 GRSS data fusion contest. IEEE Journal of Selected Topics in Applied Earth Observations and Remote Sensing, 6(3), 1324- 1340.
[21] Douillard, B., Underwood, J., Kuntz, N., Vlaskine, V., Quadros, A., Morton, P., & Frenkel, A. (2011, May). On the segmentation of 3D LIDAR point clouds. In Robotics and Automation (ICRA), 2011 IEEE International Conference on (pp. 2798-2805). IEEE.
[22]. Rodarmel, C., & Shan, J. (2002). Principal component analysis for hyperspectral image classification. Surveying and Land Information Science, 62(2), 115.
[23] Nielsen, A. A. (2011). Kernel maximum autocorrelation factor and minimum noise fraction transformations. IEEE Transactions on Image Processing, 20(3), 612-624.
[24] Wang, J., & Chang, C. I. (2006). Independent component analysis based dimensionality reduction with applications in hyperspectral image analysis. IEEE transactions on geoscience and remote sensing, 44(6), 1586-1600.
[25] Nascimento, J. M., & Dias, J. M. (2005). Vertex component analysis: A fast algorithm to unmix hyperspectral data. IEEE transactions on Geoscience and Remote Sensing, 43(4), 898-910.
[26] Nielsen, A. A. (2011). Kernel maximum autocorrelation factor and minimum noise fraction transformations. IEEE Transactions on Image Processing, 20(3), 612-624.
[27] Man, Q., Dong, P., & Guo, H. (2015). Pixel-and feature-level fusion of hyperspectral and lidar data for urban land-use classification. International Journal of Remote Sensing, 36(6), 1618-1644.
[28] Dietterich, T. G. (1998). Approximate statistical tests for comparing supervised classification learning algorithms. Neural computation, 10(7), 1895-1923.
[29] Suykens, J. A., & Vandewalle, J. (1999). Least squares support vector machine classifiers. Neural processing letters, 9(3), 293-300.
[30] Smola, A. J., & Schlkopf, B. (2004). A tutorial on support vector regression. Statistics and computing, 14(3), 199-222.
[31] Shawe-Taylor, J., & Cristianini, N. (2004). Kernel methods for pattern analysis. Cambridge university press.
[32] Kumar, S. (2004). Neural networks: a classroom approach. Tata McGraw-Hill Education.
[33] Soman, K. P., Loganathan, R., & Ajay, V. (2009). Machine learning with SVM and other kernel methods. PHI Learning Pvt. Ltd..
[34] Foody, G. M. (2002). Status of land cover classification accuracy assessment. Remote sensing of environment, 80(1), 185-201.
[35]. R. Anand, S. Veni, J. Aravinth, "An application of image processing techniques for detection of diseases on brinjal leaves using k-means clustering method", Recent Trends in Information Technology (ICRTIT) 2016 International Conference on. IEEE, 2016.
[36]. Anand, R., Veni, S., & Aravinth, J. (2017, September). Big data challenges in airborne hyperspectral image for urban landuse classification. In 2017 International Conference on Advances in Computing, Communications and Informatics (ICACCI) (pp. 1808-1814). IEEE.
[37]. Anand, R., Veni, S., & Aravinth, J. (2017, September). Big data challenges in airborne hyperspectral image for urban landuse classification. In 2017 International Conference on Advances in Computing, Communications and Informatics (ICACCI) (pp. 1808-1814). IEEE.
[38]. Shanthi, T., Sabeenian, R. S., & Anand, R. (2020). Automatic diagnosis of skin diseases using convolution neural network. *Microprocessors and Microsystems*, *76*, 103074.